University of Wisconsin
Platteville

Department of Industrial and Mechanical Engineering
725 West Main Street
Platteville, Wisconsin 53818

608. 342. 1721

COMPUTER SIMULATION FOR DYNAMIC ANALYSIS OF A DEPLOYABLE SPACE STRUCTURE

CONTRACT NO. NAS8-34506

FINAL REPORT

SEPTEMBER 1981

PREPARED BY: H. W. STOLL
ASSOCIATE PROFESSOR

PREPARED FOR: NATIONAL AERONAUTICS AND SPACE ADMINISTRATION
GEORGE C. MARSHALL SPACE FLIGHT CENTER
MARSHALL SPACEFLIGHT CENTER, ALABAMA

PREFACE

This report presents the results of a dynamic analysis of the SASP deployable structure test article currently being designed and constructed by MSFC. This study is intended to provide a theoretical component to the ongoing MSFC deployable structure development program.

Questions regarding the study or the report material should be directed to:

J. K. Harrison
National Aeronatucis and Space Administration
George C. Marshall Space Flight Center
Telephone: (205) 453-2817

OR

H. W. Stoll
University of Wisconsin-Platteville
Platteville, WI 53818
Telephone: (608) 342-1665

CONTENTS

SUMMARY

The purpose of this study was to develop a dynamic analysis of the deployment phase of the SASP deployable structure test article and to assess the deployability of the current design and suggest design modifications if necessary. The equations of motion are derived based on the principle of virtual work and are numerically integrated using a digital computer. This was a limited study effort conducted during a three month study period. Consequently, the modeling of forces, etc. was kept reasonably simple and emphasis was placed on getting the simulation up and running.

Analysis using the simulation was found to give results which make sense physically and are consistent with the conditions assumed. Usefulness of the analysis was found to be somewhat limited however, because of the excessive computer time required for multi-degree-of-freedom simulations. A scheme for partially bypassing this limitation is suggested.

Preliminary results of the analysis indicate that, in general, the deployable structure as presently designed will behave and operate as expected. It is found that some augmentation of the deployment system may be needed to assist deployment when the structure is fully compacted. Also, the analysis indicates that periods of slack deployment cable are likely to occur. Design modifcations to correct these problems are suggested and analyzed.

1.0 INTRODUCTION

For several years now NASA has pursued a program to develop the capability to build large, light-weight structures in space. Three basic building methods - space fabrication, erectable, and deployable - are generally proposed. Deployable structures appear promising for near-term applications because they do not, in general, require the formidable on-orbit construction technology necessitated by the other methods.

To develop a deployable structure design capability, NASA is designing and constructing a full scale deployable structure test article as part of the Science and Application Space Platform (SASP) program. An important concern in the design of this structure is its deployment reliability or "deployability". Ease of deployment depends on a multitude of factors such as linkage geometry, friction and manufacturing tolerances, and method of deployment to name a few.

The objective of this study is to 1) perform a kinematic and dynamic analysis of the SASP deployable structure test article and 2) assess the deployability of the current design and suggest hardware redesign to improve deployability. Because of the degree of complexity involved, the analysis has been implemented in the form of a computer simulation. This approach makes it possible to 1) thoroughly investigate the feasible design space and identify optimal design configurations; 2) investigate conditions which are too expensive or impractical using the real system; 3) investigate extreme conditions which could destroy the real system; and 4) bridge the gap between model tests and full scale hardware in cases where well defined scaling laws do not apply.

The computer simulation developed in this study has been kept relatively simple with the intent that it will help identify problem areas, provide understanding, and form the basis upon which to build a more sophisticated model.

2.0 DYNAMIC ANALYSIS

This section presents the equations of motion used to model the dynamic behavior of the SASP deployable structure test article during its deployment phase. The first step in this analysis is to formulate a kinematic model of the linkage and to select a suitable set of generalized coordinates to be used in specifying the motion of each link. Following this, the equations of motion are derived as functions of the generalized coordinates.

2.1 DESCRIPTION OF THE SASP DEPLOYABLE STRUCTURE TEST ARTICLE

A representative configuration of the SASP is shown in Figure 1. The configuration incorporates three independently oriented platform arms dedicated to celestial, solar, and earth viewing, respectively. Each platform arm provides interface provisions for payload carriers at two locations, and each location has provisions for two interfaces on opposite sides of the platform arm. Incorporated within each arm are cables which provide power and other utilities to the payloads. The platform arms utilize deployable structures which permit longitudinal compaction of the arm for launch in the Orbiter cargo bay.

The SASP deployable structure test article is a full-scale prototype version of one of the SASP platform arms. It is equipped with utility cables and payload carrier interfaces and is intended to serve as a test bed for development of the SASP platform arm deployable structure. The SASP deployable structure test article is depicted schematically as a planar mechanism in Figure 2. Although the platform arm is a three-dimensional structure, it can be treated as a two-dimensional planar mechanism for purposes of kinematic and dynamic analysis. This is because the structure folds and deploys in the longitudinal direction only.

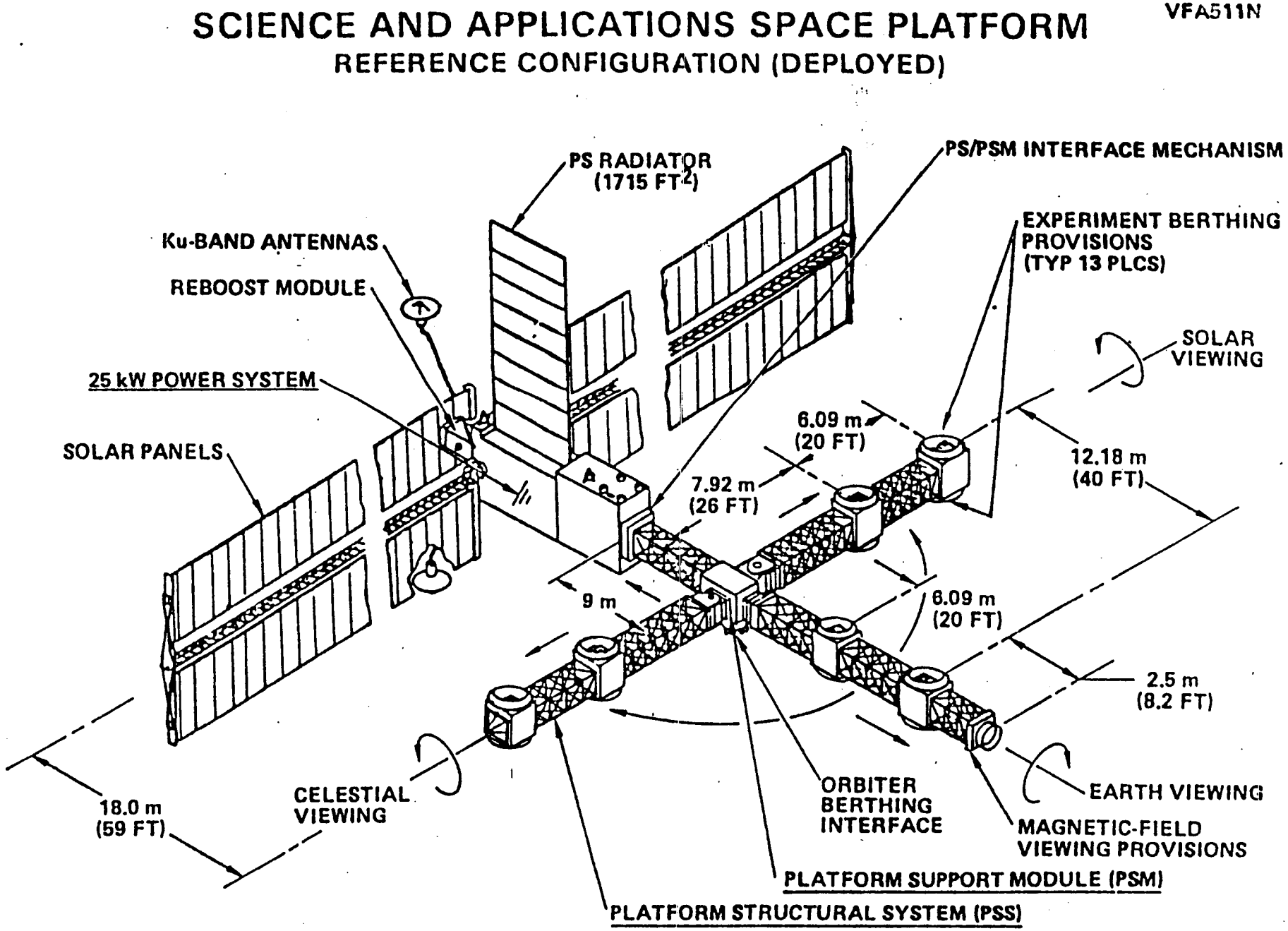

Figure 1. Science and Applications Space Platform

As can be seen in Figure 2, the test article consists of a series of ten simple parallelogram linkages connected, one after the other, in such a way that each linkage forms one bay of the ten bay deployed structure. Each bay is 55.0 inches long by 55.0 inches high by 55.0 inches wide. The sixth and tenth bays from the fixed end of the structure provide payload carrier interfaces. It should be noted that, because of the payload carrier interfaces and other design details, there is significant variation in link properties from bay to bay.

Each bay is converted from a linkage to a structure by a set of telescoping diagonal members which are "rigidized" upon full deployment. Although there are actually two telescoping members per bay, one on either side of the structure, kinematically they can be treated as a single telescoping member since the motion of both diagonals must be identical for the linkage to move as a whole. This simplification makes it possible to view each bay as consisting of 5 links. These are the upper and lower longeron links, the coupler link, and the two concentric links which form the telescoping diagonal.

Deployment of the structure is facilitated by cables threaded through the telescoping diagonal links located on either side of the structure. The cables wrap around pulleys mounted on each coupler link and produce deployment motion by exerting force on the coupler links as the cables are reeled in by a winch device located at the fixed end of the structure.

An important feature of the design is the offset built into each coupler link. This offset allows the structure to be folded so that all links are parallel when the structure is fully compacted as shown schematically in Figure 3. Note that in this position, the longeron and coupler links are aligned in a straight line. During deployment, the telescoping links

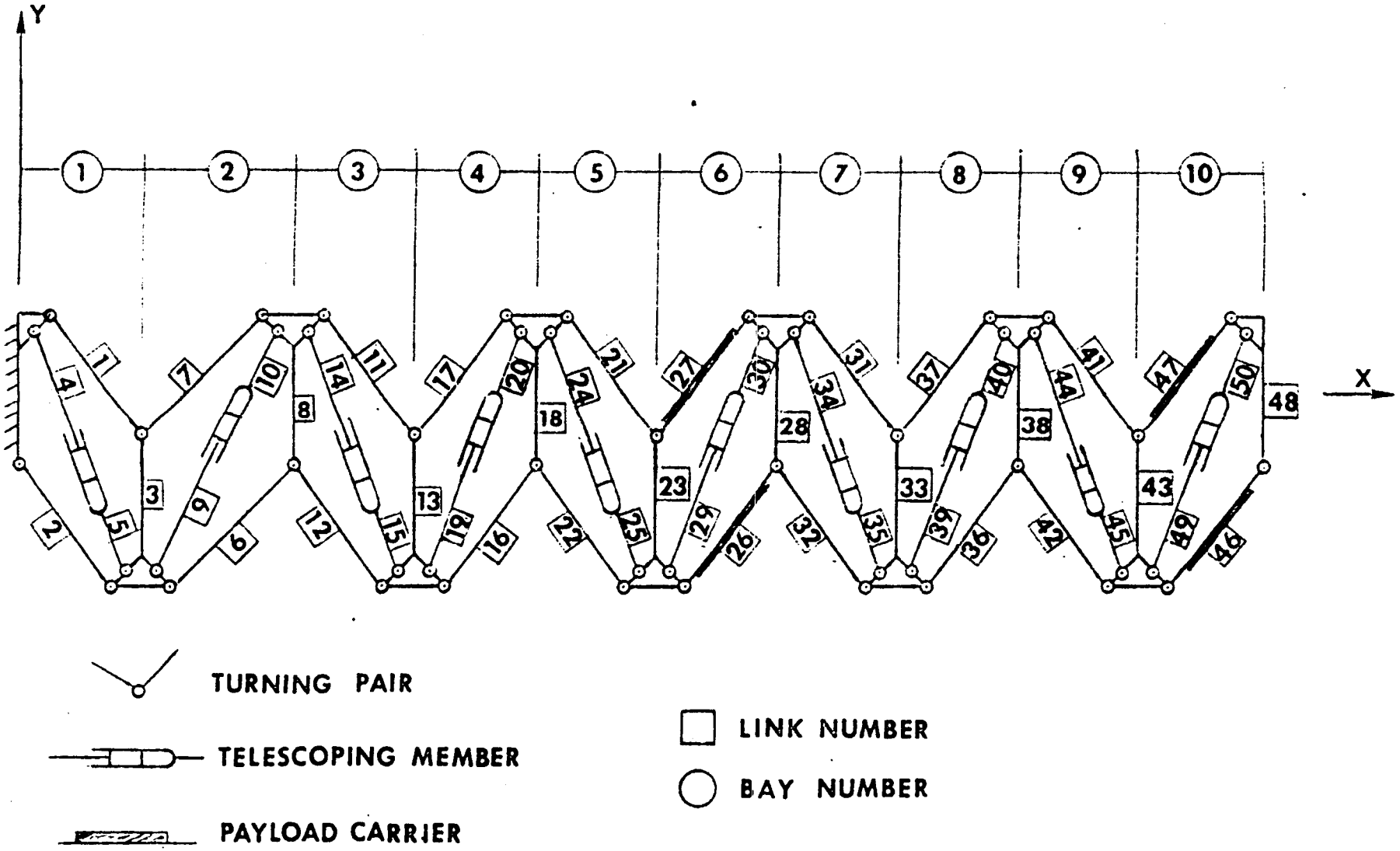

Figure 2. SASP Deployable Structure Test Article

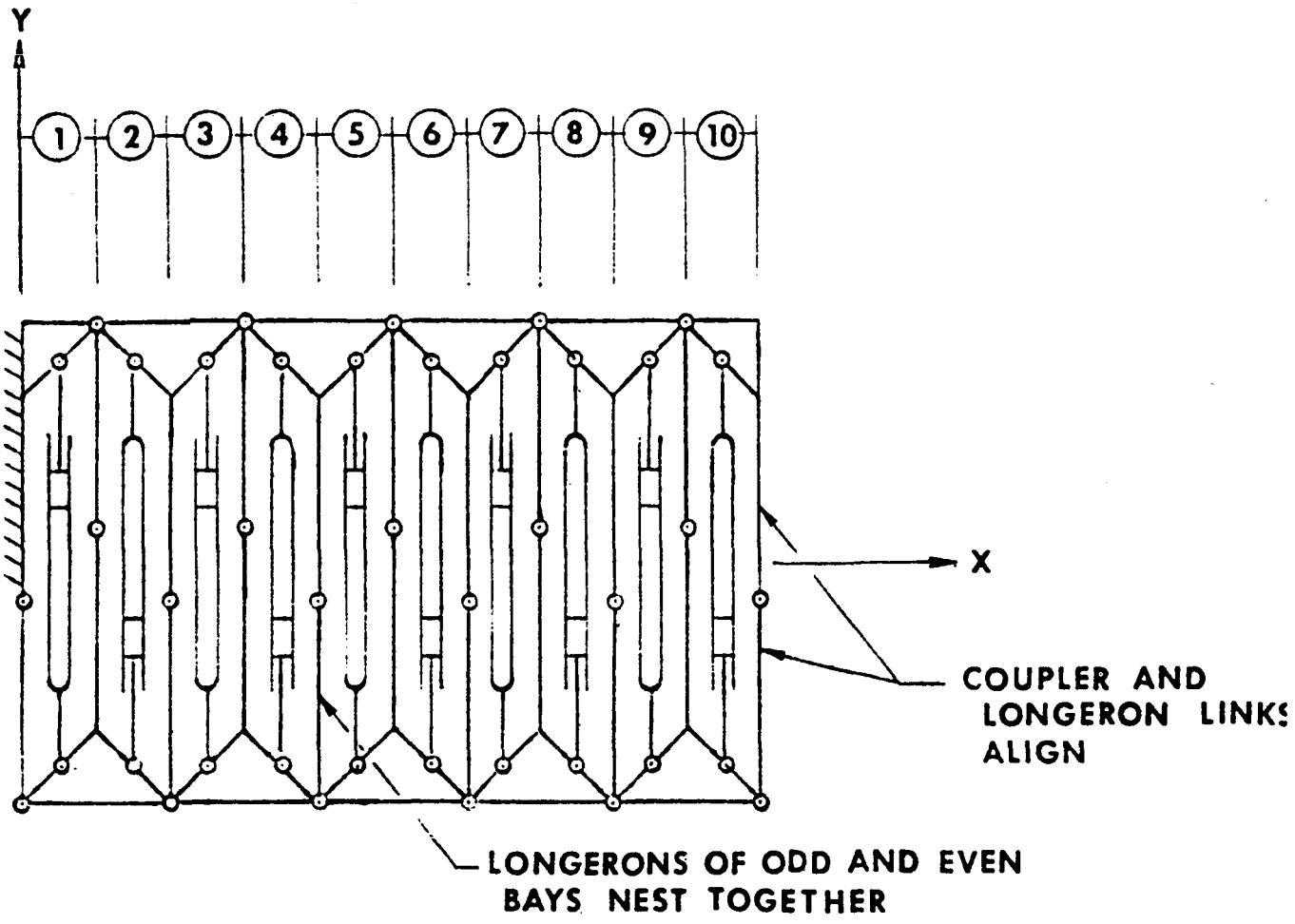

Figure 3. Fully Compacted Structure

contract and the longeron links rotate from the aligned position of Figure 3 to the fully deployed position. When fully deployed, the longeron and coupler links are at 90° to each other. Because the upper and lower longerons are equal in length, the coupler link translates but does not rotate during deployment.

Several aspects of this deployment scheme need further discussion. First, in the fully compacted position of Figure 3, no deployment motion can be imparted to the linkage using the cable deployment scheme. This is because the longeron and coupler links are aligned and hence, for this "singular" position, the longerons become loaded in compression without a turning moment as the cable is pulled in. Consequently, either sufficient

cable force must be applied to cause the aligned links to buckle, or auxiliary deployment mechanisms such as "break-out" springs are needed to initiate deployment.

A second consideration involves the possibility of slack developing in the deployment cables once the linkage is in motion. Slack will occur if the combined velocity of contraction of the telescoping links exceeds the "haul-in" rate of the winch. Slack in the deployment cable system is highly undesireable since it can lead to jamming of the linkage, derailment of the cable from its pulleys, and excessive impact loading of linkage and cable components.

Finally, it should be noted that the deployment scheme employed produces "quasi-simultaneous" deployment of all bays. This leads to complicated couplings and dynamic interactions between each bay. For this reason, even if highly simplified mathematical models of the linkage are employed, it is very difficult to predict the deployment behavior of the structure as a whole using closed form analysis. When the high degree of variability in link inertia properties from bay to bay, intermittent action of break-out springs and other devices, and the highly non-linear nature of the different equations of motion are considered together, it becomes very obvious that numerical integration of the equation of motion using the digital computer is the only viable approach to dynamic analysis of the deployment phase.

2.2 KINEMATIC MODEL

The kinematic model of the deployable linkage is depicted graphically in Figure 2 with detail dimensional nomenclature defined for one bay in Figure 4. As shown in Figure 2, the x-y axis defines the plane of motion. The origin of the x-y axes is symmetrically located at the fixed end of the structure and is oriented such that, when fully deployed, the longitudinal

centroidal axis of the structure coincides with the x-axis.

Each bay is numbered sequentially, beginning with bay 1 at the fixed end of the structure and proceeding to bay 10 at the free end of the structure. Bays 6 and 10 provide payload carrier interfaces. Since there are 10 bays in the structure with 5 links per bay, a total of 50 links must be accounted for in the model. The motion of each link is defined by that of a characteristic edge embedded in the link. These characteristic edges are numbered sequentially from 1 to 50 as shown by the numbers enclosed with small squares in Figure 2.

Mobility analysis of the deployable linkage shows that one coordinate is required to define the motions of the links of each bay. Hence, the system has as many degrees-of-freedom as there are bays. Although a number of different coordinates could be chosen, the angular position of the longerons of each bay was selected since it is felt that these coordinates convey the most immediate information regarding the deployment status of the linkage. The set of independent generalized coordinates $(\theta_1, \theta_2, \ldots, \theta_{10})$ are defined as shown in Figure 4 and are measured relative to the fixed set of global (x, y) axes. Because of the alternating folding arrangement of the structure, it is seen that the range of variability of the generalized coordinates is

$$270° \leq \theta_r \leq 0 \quad \text{for } r = 1, 3, 5, 7, 9$$

and

$$0 \leq \theta_r \leq 90° \quad \text{for } r = 2, 4, 6, 8, 10$$

where the index r denotes bay number.

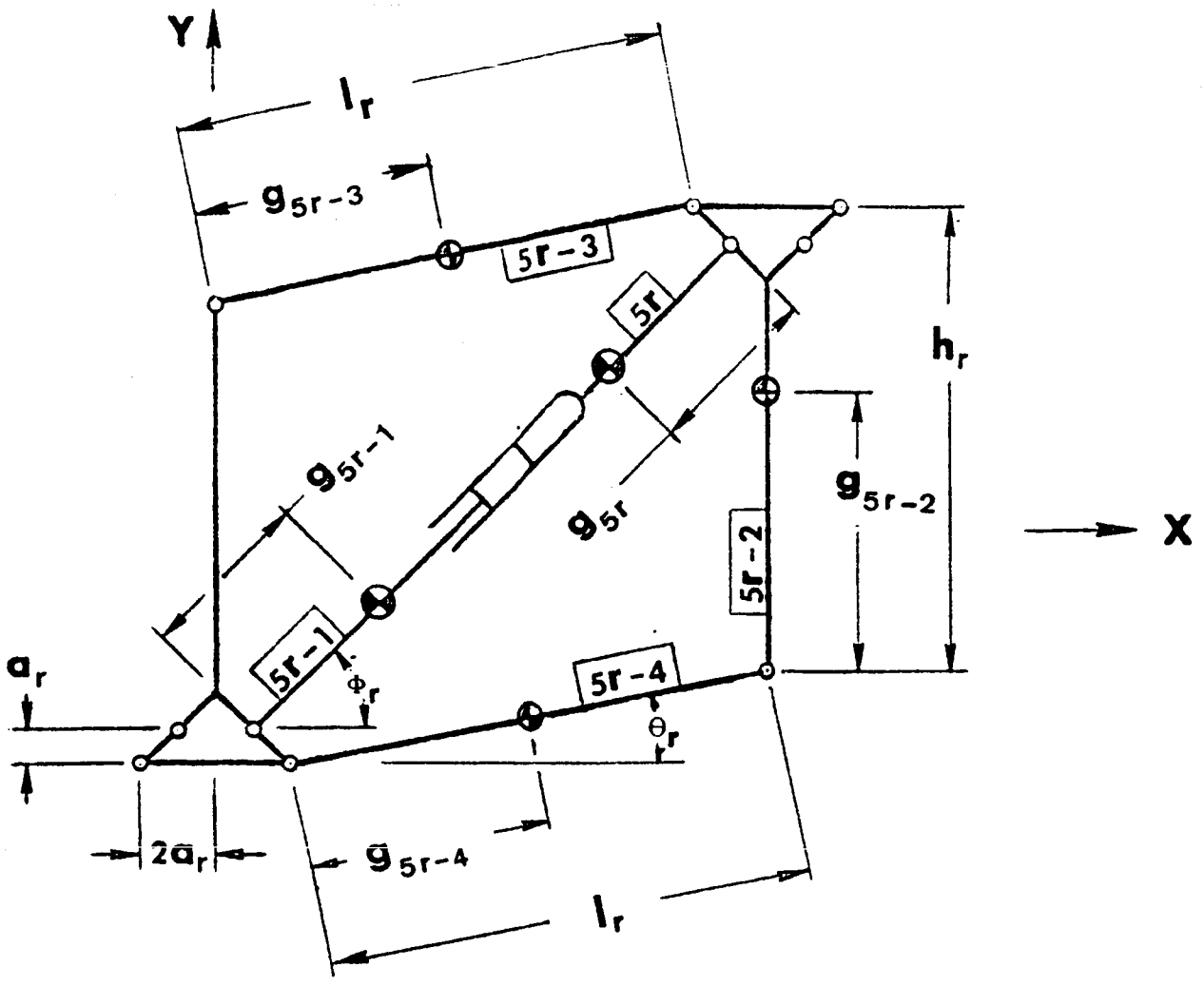

Figure 4. Kinematic Model for a Typical Bay

Letting i denote link number and utilizing the fact that the link configuration of each bay is similar, it is convenient to relate link and bay number by the relation

$$i = 5r - k + 1 \qquad \begin{cases} k = 1, 2, 3, 4, 5 \\ r = 1, \ldots, 10 \end{cases}$$

An example of the use of this relation is the numbering of links for the typical bay of Figure 4. Later on, this relation is widely utilized both in the equations of motion and in the computer coding.

Each link has a mass m_i concentrated at its center of mass (C.M.) and a mass moment of inertia J_i about its C.M. The C.M. for each link is located by g_i measured as shown in Figure 4. All active* forces acting on each link

* Active forces are defined as forces which do non-zero virtual work.

are combined into a set of Cartesian force components (X_i, Y_i, M_i) acting through and about the C.M.

The C.M. of each link is located relative to the global (x,y) axis by the Cartesian coordinates x_i, y_i. Angular orientation of the characteristic edge of each link is given by the angle ψ_i measured counter clockwise from the positive x-axis. First and second derivatives of these variables with respect to time are denoted as $\dot{x}_i$, $\dot{y}_i$, $\dot{\psi}_i$ and $\ddot{x}_i$, $\ddot{y}_i$, $\ddot{\psi}_i$ respectively. Since conceptually, any number of bays can be used, in the equations that follow, F is used to denote the total number of bays and n denotes the total number of links. It should also be noted that n = 5F due to the repetitive nature of each bay.

2.3 EQUATIONS OF MOTION

Derivation of the equations of motion for the deployable linkage of Figure 2 is based on d'Alembert's Principle using the method of virtual work [1]*. This leads to the general equation of dynamics which can be expressed as [2],

$$\sum_{i=1}^{n} [(X_i - m_i\ddot{x}_i)\dot{x}_i + (Y_i - m_i\ddot{y}_i)\dot{y}_i + (M_i - J_i\ddot{\psi}_i)\dot{\psi}_i] = 0 \qquad (1)$$

Equation (1) holds for any set of velocities ($\dot{x}_i$, $\dot{y}_i$, $\dot{\psi}_i$) that is compatible with the kinematic constraints imposed by the deployable linkage configuration. To ensure that the velocities ($\dot{x}_i$, $\dot{y}_i$, $\dot{\psi}_i$) are compatible with the constraints, they are expressed in terms of the generalized coordinates (θ_1, θ_2,..., θ_F). These kinematic relations are summarized as follows:

* numbers in brackets denote references at the end of the report

$$\{\dot{x}_i, \dot{y}_i, \dot{\psi}_i\} = \sum_{r=1}^{F} \{U_{ir}, V_{ir}, \Omega_{ir}\} \dot{\theta}_r \qquad (2)$$

where

$$U_{ir} = \begin{cases} -l_r \sin\theta_r & , i > 5r \\ -(g_i\omega_i + l_r c_i)\sin\theta_r & , (5r-4) \leq i \leq 5r \\ 0 & , i < (5r-4) \end{cases}$$

$$V_{ir} = \begin{cases} l_r \cos\theta_r & , i > 5r \\ (g_i\omega_i + l_r c_i)\cos\theta_r & , (5r-4) \leq i \leq 5r \\ 0 & , i < (5r-4) \end{cases}$$

$$\Omega_{ir} = \begin{cases} 0 & , i > 5r \\ \omega_i & , (5r-4) \leq i \leq 5r \\ 0 & , i < (5r-4) \end{cases}$$

and $\omega_i = 1$ for $i = 5r - k + 1$ $\begin{cases} k = 4, 5 \\ r = 1, \ldots, F \end{cases}$

$\omega_i = 0$ for $i = 5r - 2$, $r = 1, \ldots, F$

$\omega_i = l_r \cos(\phi_r - \theta_r)/s_r$ for $i = 5r - k + 1$ $\begin{cases} k = 1, 2 \\ r = 1, \ldots, F \end{cases}$

$c_i = 0$ for $i = 5r - k + 1$ $\begin{cases} k = 2, 4, 5 \\ r = 1, \ldots, F \end{cases}$

$c_i = 1$ for $i = 5r - k + 1$ $\begin{cases} k = 1, 3 \\ r = 1, \ldots, F \end{cases}$

$\phi_r = \tan^{-1}[\tan\theta_r - K_r]$, $r = 1, 3, 5, 7, 9, \ldots$

$\phi_r = \tan^{-1}[\tan\theta_r + K_r]$, $r = 2, 4, 6, 8, 10, \ldots$

$s_r = l_r \cos\theta_r / \cos\phi_r$, $r = 1, \ldots, F$

$K_r = (h_r - 2a_r)/(l_r \cos\theta_r)$, $r = 1, \ldots, F$

Differentiating equation (2) with respect to time gives

$$\{\ddot{x}_i, \ddot{y}_i, \ddot{\psi}_i\} = \{U_i, V_i, \Omega_i\} + \sum_{j=1}^{F} \{U_{ij}, V_{ij}, \Omega_{ij}\} \ddot{\theta}_j$$

where $\{U_i, V_i, \Omega_i\} = \sum_{r=1}^{F} \{\dot{U}_{ir}, \dot{V}_{ir}, \dot{\Omega}_{ir}\} \dot{\theta}_r^2$, $i = 1, 2, \ldots, n$ (3)

and $\dot{U}_{ir} = \begin{cases} -V_{ir} \dot{\theta}_r & , i > 5r \\ -[g(g_i\omega_i + l_r c_i) \cos \theta_r - g_i\omega_i' \sin \theta_r], & (5r-4) \leq i \leq 5r \\ 0 & , i < (5r-4) \end{cases}$

$\dot{V}_{ir} = \begin{cases} U_{ir} \dot{\theta}_r & , i > 5r \\ -[(g_i\omega_i + l_r c_r) \sin \theta_r - g_i\omega_i' \cos \theta_r] & , (5r-4) \leq i \leq 5r \\ 0 & , i < (5r-4) \end{cases}$

$\Omega_{ir} = \begin{cases} 0 & , i > 5r \\ \omega_i' & , (5r-4) \leq i \leq 5r \\ 0 & , i < (5r-4) \end{cases}$

$$\omega_i' = 0 \text{ for } i = 5r - k + 1 \begin{cases} k = 3, 4, 5 \\ r = 1, \ldots, F \end{cases}$$

$$\omega_i' = -\frac{l_r}{5r} [(\omega_i - 1) + \frac{l_r}{5r} \cos (\phi_r - \theta_r)] \sin (\phi_r - \theta_r)$$

$$\text{for } i = 5r - k + 1 \quad \begin{cases} k = 1, 2 \\ r = 1, \ldots, F \end{cases}$$

Substituting equations (2) and (3) into equation (1) gives

$$\sum_{i=1}^{n} \sum_{r=1}^{F} [(X_i U_{ir} + Y_i V_{ir} + M_i \Omega_{ir}) - (m_i U_i U_{ir} + m_i V_i V_{ir} + J_i \Omega_i \Omega_{ir}) - \sum_{j=1}^{F} (M_i U_{ij} U_{ir} + m_i V_{ij} V_{ir} + J_i \Omega_{ij} \Omega_{ir}) \ddot{\theta}_j] \dot{\theta}_r = 0 \quad (4)$$

By summing over the index i and then over index r, equation (4) can be made to assume the form

$$\sum_{r=1}^{F} (Q_r - C_r - \sum_{j=1}^{F} I_{rj}\ddot{\theta}_j)\,\dot{\theta}_r = 0 \qquad (5)$$

where $Q_r = \sum_{i=1}^{n} (X_i U_{ir} + Y_i V_{ir} + M_i \Omega_{ir})$

$$C_r = \sum_{i=1}^{n} (m_i U_i U_{ir} + m_i V_i V_{ir} + J_i \Omega_i \Omega_{ir})$$

$$I_{rj} = \sum_{i=1}^{n} (m_i U_{ij} U_{ir} + m_i V_{ij} V_{ir} + J_i \Omega_{ij} \Omega_{ir})$$

Examination of equation (5) shows that the quantities Q_r are the generalized forces acting on the linkage; the quantities C_r represent inertia forces due to centripetal and Coriolis accelerations; and the coefficients I_{rj} satisfy the symmetry relation $I_{rj} = I_{jr}$ and form the elements of a symmetric square matrix which can be thought of as a generalized inertia matrix [2]. Now, since equation (5) must be valid for every possible combination of generalized velocities $\dot{\theta}_r$, it must hold for the particular set

$$\dot{\theta}_1 = 1,\ \dot{\theta}_r = 0\ (r \neq 1).$$

When this condition is substituted into equation (5), the only surviving terms are

$$\sum_{j=1}^{F} I_{1j}\ddot{\theta}_j = Q_1 - C_1.$$

Similarly, by letting

$$\dot{\theta}_s = 1,\ \dot{\theta}_r = 0,\ (r \neq s)$$

where s is any integer in the range 1, 2, ..., F, equation (5) reduces to

$$\sum_{j=1}^{F} I_{sj}\ddot{\theta}_j = Q_s - C_s,\ s = 1, 2, \ldots, F \qquad (6)$$

Equations (6) represent a set of F differential equations, each of second order in the generalized coordinate θ_j. These equations of motion describe the dynamic behavior of the deployable linkage of Figure 2 and form the basis for a computer simulation of the deployment phase.

2.4 MODELING OF FORCES

The deployable linkage of Figure 2, when considered in its entirety, is an extremely complex mechanism whose operation will involve the action of a wide variety of forces and moments. Forces will arise due to the action of the deployment system, resistance to relative motion of the pinned joints and sliding elements, drag of the utility cable, and weight of the links to name a few. In addition, there is friction in the cable run and telescoping members, forces arising due to link misalignment and deflection, and the variability of these effects from link to link and bay to bay to be considered. When these complexities are combined with the complexities created by the ten degrees-of-freedom inherent in the mechanism, it is seen that accuracy of the dynamic analysis may be highly dependent on how correctly these forces are modeled.

As stated previously, the analysis developed in this study has been kept relatively simple in order to get the computer simulation up and operating in the short time available. Accuracy and correctness of this simplified approach will become evident when the full-scale testing of the test article at Marshall is begun. A summary of the forces modeled and assumptions used in the present analysis is given in the following paragraphs.

Deployment Forces. Deployment forces are applied to the coupler link of each bay as the actuation cable is "hauled-in". These forces are shown schematically in Figure 5 for a typical coupler link of bay r. Forces acting at the center of mass of the link are

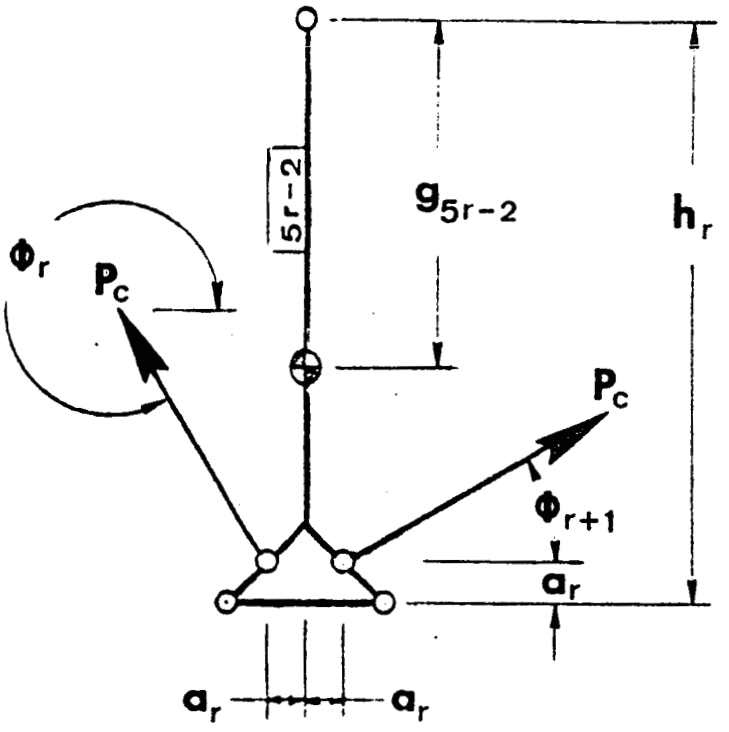

Figure 5. Deployment Forces Acting on a Typical Coupler Link

$$X_{5r-2} = -P_c \cos \phi_r + P_c \cos \phi_{r+1}$$

$$X_{5r-2} = -P_c \sin \phi_r + P_c \sin \phi_{r+1} \qquad r = 1, \ldots, F-1$$

$$X_{5F-2} = P_c \cos \phi_F$$

$$X_{5F-2} = P_c \cos \phi_F \qquad r = F$$

$$M_{5r+2} = X_{5r-2} (h - g_{5r-2} - a) \qquad r = 1, \ldots, F$$

where P_c is the tension in the deployment cable and X, Y, and M cut through and about the C.M. of the link.

Tension in the deployment cable, P_c, is developed as the deployment cable stretches due to the reeling-in action of the winch. This force can be modeled as

$$P_c = K_{cable} [v_{cable}\, t - S_o + S_t]$$

where $K_{cable} = \frac{\pi E_{cable} d_{cable}^2}{4 S_t}$ = spring rate of cable

E_{cable} = Modules of elasticity of cable

d_{cable} = diameter of cable = 3/16 inch

t = time

$S_t = \sum_{i=1}^{F} S_r$ at time = t

$S_o = \sum_{r=1}^{F} S_r$ at time = 0

and v_{cable} = haul-in rate of winch

Assuming that the winch can maintain v_{cable} without stalling, high cable tensions can develop due to the dynamics of the system. Also, due to dynamics of the system, velocities in the linkage can be such that

$$[v_{cable}\, t - S_o + S_t] < 0,$$

which will lead to a slack cable condition. To deal with these extremes, the following checks are applied to the calculated value of P_c,

IF $(P_c > P_{max})$ THEN $P_c = P_{max}$

IF $(P_c < 0)$ THEN $P_c = 0$

Letting $P_c = P_{max}$ when $P_c > P_{max}$ represents the action of a load limiting slip clutch. When this check is invoked, the take up velocity is assumed to be reduced such that

$$v_{cable}\, t = \frac{P_{max}}{K_{cable}} + S_o - S_t.$$

By setting the value of P_{max} sufficiently high, (e.g., > 10,000 lbs), the effect of this load limitation scheme can be eliminated from the simulation.

When the $P_c < 0$ check is invoked, the cable is assumed to be slack. No forces due to bunching up of the cable or jamming of the links have been modeled. During the slack cable condition, cable take-up is assumed to continue at the constant rate v_{cable}.

Torsional "break-out" springs are also included to supply deployment torque to the longeron links. The breakout springs are required because the cable deployment system by itself will not initiate deployment motion of the fully compacted structure. Action of the breakout springs are modeled as

$$M_{5r-4} = M_{5r-3} = \begin{cases} K_{brk}(\theta_{el} - \theta_r), & \theta_r < \theta_{el} \\ 0, & \theta_r < \theta_{el} \end{cases} \qquad r = 1,3,5,7,9$$

$$M_{5r-4} = M_{5r-3} = \begin{cases} K_{brk}(\theta_r - \theta_{e2}), & \theta_r > \theta_{e2} \\ 0, & \theta_r < \theta_{e2} \end{cases} \qquad r = 2,4,6,8,10$$

where θ_{el}, θ_{e2} are the engagement angles for the odd and even bays respectively and K_{brk} is the torsional spring rate of the springs. It is assumed that K_{brk} and θ_{el}, θ_{e2} are the same for each bay.

Turning and Sliding Pair Forces. All turning pairs in the linkage are considered to have constant resistance to relative motion between the pair elements. This is expressed as

$$M_i = -kT_{joint} \operatorname{sgn} \theta_r$$

where k refers to the number of joints per link, T_{joint} is the resistive torque, and - sgn θ_r indicates that the joint torque opposes the rotation of the link.

The telescoping members were modeled as viscous dampers. Since the telescoping members connect to the coupler links (see Figures 2, 4, 5), this damping force is given as

$$\left.\begin{aligned} X_{5r-2} &= -\zeta_d S_r \cos \phi_r + \delta_d S_{r+1} \cos \phi_{r+1} \\ Y_{5r-2} &= -\zeta_d S_r \sin \phi_r + \delta_d S_{r+1} \sin \phi_{r+1} \end{aligned}\right\} \quad r = 1,\ldots,F-1$$

$$\left.\begin{aligned} X_{5r-2} &= -\zeta_d S_r \cos \phi_r \\ Y_{5r-2} &= -\zeta_d S_r \sin \phi_r \end{aligned}\right\} \quad r = F$$

$$M_{5r-2} = X_{5r-2}\, g_{5r-2}, \qquad r = 1,\ldots,F$$

where $\dot{S}_r = l_i \sin (\phi_r - \theta_r)\, \dot{\theta}_r$

and ζ_d is the damping constant which is assumed the same for all telescoping links.

Utility Cable Forces. The utility cable is modeled as a constant force spring (zero spring rate) which applies drag to each coupler link in both the x and y directions, i.e.,

$$\begin{aligned} X_{5r-2} &= X_{util} \operatorname{sgn} x_{5r-2} \\ Y_{5r-2} &= Y_{util} \operatorname{sgn} y_{5r-2} \end{aligned} \qquad r = 1,\ldots,F$$

Hence, if X_{util}, Y_{util} are given negative signs, they apply a drag to the coupler link which hinders its deployment. If X_{util}, Y_{util} are given positive signs, the utility cable tends to promote deployment of the coupler link. X_{util}, Y_{util} are assumed to be the same for each bay.

Link Weight. Weight of each link is modeled as

$$X_i = m_i g_c \cos \alpha \cos \beta$$

$$Y_i = m_i g_c \sin \alpha \cos \beta$$

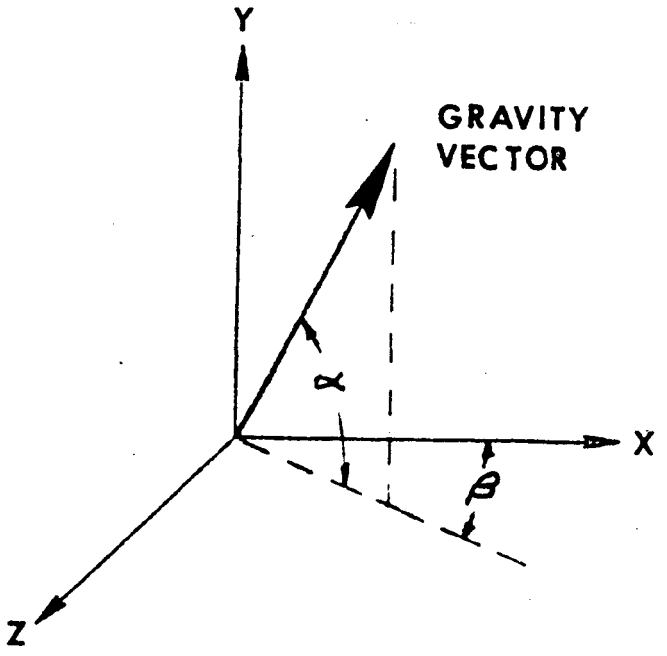

Figure 6. Orientation of Gravity Vector

where the angles α and β are defined as shown in Figure 6 and the x-y plane defines the plane of deployment motion. Hence, for the full scale hardware tests, the x-y plane will be horizontal, i.e., $\alpha = 0$, and $\beta = 90°$, and it is seen that link weights will neither directly hinder or promote deployment of the structure. Orientation of the structure with respect to gravity is easily controlled in the simulation by specifying the angles α and β. The zero g condition is simulated by setting the graviational constant, g_c, equal to zero.

Locking Mechanism. Once a bay has fully deployed ($\theta_r = 0$), a latch on the diagonal link engages preventing further motion of the bay. This latching action is modeled by the following equations:

Latch = 0

If ($S_r < S_f$) then Latch = 1

$$\text{If } (S_r < S_f) \begin{cases} X_{5r-2} = K_{lock} (S_f - S_r) \cos \phi_r \\ Y_{5r-2} = K_{lock} (S_f - S_r) \sin \phi_r \end{cases} \Bigg\} r = 1, \ldots, F$$

$$\text{If } (S_r > S_f \text{ and latch} \neq 0) \begin{cases} X_{5r-2} = -K_{lock} (S_r - S_f) \cos \phi_r \\ Y_{5r-2} = -K_{lock} (S_r - S_f) \sin \phi_r \end{cases}$$

All the forces discussed above are computed and combined into a set of Cartesian forces components (X_i, Y_i, M_i) acting through and about the C.M.

of each link by the subroutine FORCES.

2.5 LINK PROPERTIES

Expressions for link properties including weight, mass (m_i), location of center of mass (g_i), and mass moment of inertia (J_i) were formulated in terms of longeron length (l_i), and deployed structure height (h) and width (W). The relationships are based on detail drawings of the full-scale test article as supplied by MSFC. Since the link properties are primarily dependent on the l_i, h, and W dimensions, these equations permit approximate scaling of link properties over a range of values for l_i, h, W. These expressions are accurate for the full scale hardware. Accuracy diminishes as l_i, h, and W are made smaller since these dimensions become less dominant. Accuracy of the equations should remain relatively good for reasonable increases in l_i, h, or W since they become more dominant in the calculations. The property relations have been coded in Subroutine PROPER. Numerical values for the full-scale link properties as computed using Subroutine PROPER are tabulated in Table 1.

Table 2.5-1

Link Properties for Full Scale Hardware
(l = 51.0, H = 55.0, W = 55.0 in., p = .098 lb/in^3)

Link Numbers	Weight (lbs)	Mass, m_i (lb-sec^2-in)	Mass Moment of Inertia, J_i, (lb-sec^2-in)	Center of Mass Location**, g_i (in)
Longeron Link Numbers 1, 2, 11, 12, 21, 22, 31, 32, 41, 42	8.3	0.0216	4.762	25.146
Longeron Link Numbers 6, 7, 16, 17, 36, 37	9.1	0.2344	5.108	35.016
Longeron Link Numbers (payload in surfaces)	51.5	0.1334	31.008	37.258
Coupler Links 3, 8, 13, 18, 23, 28, 33, 38, 45, 48	9.0	0.0233	18.853	32.144
Diagonal Link Numbers 4, 9, 14, 19, 24, 29, 34, 39, 40, 49	4.2*	0.0108*	4.050*	25.423
Diagonal Link Numbers 5, 10, 15, 20, 25, 30, 35, 40, 45, 50	2.8*	0.0074*	1.608*	26.460

* Value is combined value for both diagonal links

** See Figure 4.

2.6 NUMERICAL INTEGRATION OF THE EQUATIONS OF MOTION

The initial value problem formulated can be solved by numerical integration by first converting the second order differential equations (6) into two first-order equations with the aid of the auxiliary variables

$$\{\theta_1, \theta_2, \ldots, \theta_r\} = y_1, y_2, \ldots y_r \tag{7}$$

$$\{\dot{\theta}_1, \dot{\theta}_2, \ldots, \dot{\theta}_r\} = y_{F+1}, y_{F+2}, \ldots, y_{2r} \tag{8}$$

Then the equations of motion (6) can be expressed in the form

$$\sum_{j=1}^{F} I_{sj} \ddot{y}_{F+j} = Q_s - C_s \quad (s = 1, 2, \ldots, F) \tag{9}$$

With the initial values of θ_r and $\dot{\theta}_r$ known, all the secondary variables (s_r, ϕ_r, x_i, y_i, ψ_i) can be determined since all have been expressed previously as explicit functions of θ_r and $\dot{\theta}_r$. Hence, the terms I_{sj}, Q_s, and C_s, which appear in equation (9) can be evaluated and the linear equation (9) can be solved for the initial values of y_{F+j}. Moreover, this procedure can be repeated at any stage of the solution where displacements (θ_r) and velocities ($\dot{\theta}_r$) are known. In short, equation (9) can be written in symbolic form

$$y_{F+p} = F_p [y_1, y_2, \ldots, y_{2F}] \quad (p = 1, \ldots, F) \tag{10}$$

to express the fact that y_{F+p} can be calculated from $y_1, \ldots, y_{2F}$. If equation (8) is rewritten in the form

$$\dot{y}_r = \dot{\theta}_r = y_{F+r} \quad (r = 1, \ldots, F) \tag{11}$$

it is seen that $\dot{y}_1, \dot{y}_2, \ldots, \dot{y}_{2F}$ may all be formed from equations (10) and (11) for known values of $y_1, \ldots, y_{2F}$. Hence, equations (10) and (11) represent a system of differential equations of order 2F in standard form for numerical integration.

Therefore, a Runge-Kutta (or equivalent) routine can be called to solve for the updated values ($y_1, \ldots, y_{2F}$) at time $t + \Delta t$. Once these are known, all other position and velocity variables can be determined. Hence, all of the state variables become known at time $t + \Delta t$ which may now be regarded as a new initial time. All of the above steps are then repeated to find $y_1, \ldots, y_{2F}$ at time $t + 2\Delta t$. The process may be repeated over the entire range of interest ($0 \leq t \leq t_{max}$).

Initially, equations (10) and (11) were integrated using the fourth-order Runge-Kutta algorithm with Gill's coefficients as implemented in the IBM subroutine DRKGS [3]. However, it was found that very small step sizes (e.g., 0.005 sec. or less) were required to provide convergence. This, combined with the large number of function evaluations required by this approach and the excessive computer time required per function evaluation (especially when F = 10) made this approach impractical from a computer time standpoint.

Several alternative integration methods were then tried, with Hamming's Method [4] finally being chosen for use in the simulation. This method was chosen primarily because it can be modified such that only two function evaluations are required per step. The equations for the method as needed in this analysis are given in ref. [5]. Since Hamming's method is a predictor-corrector method, the subroutine DRKGS is used to start the integration procedure.

2.7 COMPUTER IMPLEMENTATION

The equations of motion for the deployable linkage of Figure 2 were coded in double precision using Fortran IV for numerical evaluation using an IBM 4331 digital computer. A main program called DSDSS (Dynamic Simulation of Deployable Space Structures) is used to input linkage properties, initial conditions, simulation conditions, and loading conditions. In addition, DSDSS carries out the numerical integration of the equations of motion.

During the course of the integration procedure, program DSDSS calls upon subroutine PROPER to provide link property data; subroutine DRKGS to provide

starting values for the predictor-corrector integration scheme; subroutine FCT to evaluate all terms of the equations of motion and put them in standard form for numerical integration; and subroutine OUTP which determines the arrangement of output. Subroutine FCT in turn, calls upon subroutine POSIN to provide link position data; subroutine FORCES to provide the forces acting through and about the center of mass of each link and subroutine DGELG which solves the system of linear equations using Gauss elimination with complete pivoting. The organization of main and subprograms is shown in Figure 7.

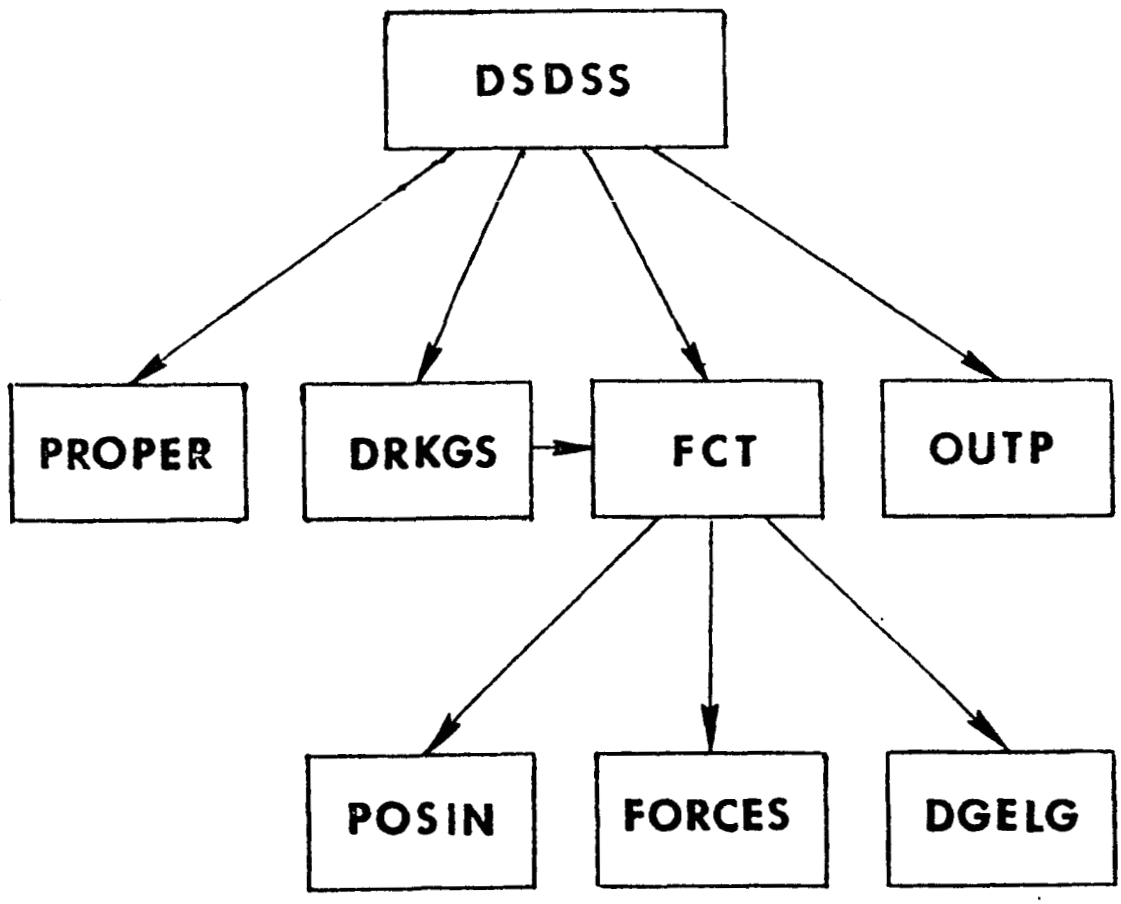

Figure 7. Relationship of main program DSDSS to subroutines. Arrows point from calling program to called programs.

Documented listings of DSDSS, PROPER, FCT, POSIN, FORCES, and OUTP are available upon request. Listings for DRKGS and DGELG are standard IBM

subroutines and are fully documented in ref. [3].

The deployable linkage of Figure 2 was also programmed for graphical display on a Tektronix 4051 graphics terminal. This program utilizes successive sets of coordinates θ_r generated by the simulation to display a series of pictures of the linkage as it deploys. This is useful in providing visual interpretation of the simulation data.

2.8 DESIGN ANALYSIS USING THE SIMULATION

As mentioned previously, the computer time required to carry out a simulation run is excessive. This problem is caused by the small time step size needed for convergence of the numerical integration and by the computationally complex nature of the equations of motion. The small step size limitation results from the non-linear nature of the equations, the complex couplings between equations, and the wide variation in link properties for each bay and from bay to bay (see Table 1). A general rule of thumb states that the step size should be on the order of one-tenth of the fundamental natural period of the system. If one coupler link ($m = 0.0233$ lb-sec^2/in) acting in conjunction with the two 1,020 inch long by 3/16 diameter deployment cables (k 650 lb/in) is considered as a simple spring-mass system, the natural period is found to be 0.006 seconds. In view of this, the 0.005 second maximum step size required by the simulation appears to be fairly well fixed by the numerical size of the physical properties involved.

On the other hand, several measures can be taken to improve the computational efficiency of the function evaluation. First, it is likely that some improvements can be gained by paying close attention to the numerical procedures used in evaluating the equations of motion. For example, a more economical

equation solving method such as Cholisky's (Crout's) method [5] could be used in place of the Gauss elimination method presently employed. Secondly, the use of a large word, high speed computer such as the UNIVAC is likely to reduce computation time significantly compared to the relatively slow IBM 4331 used in the present study.

Finally, computation time can be significantly reduced by limiting the number of bays (degree-of-freedom) considered. This is because the amount of numerical computation required increases exponentially as the number of bays is increased. In addition, increasingly large systems of equations must be solved as the number of freedoms is increased. In view of this, the following four-step scheme is recommended for using the simulation as a design tool.

1. Conduct parametric studies initially using only one bay. Use both bays 4 and 6 in these studies since they contain the extremes in link properties.

2. Modify the results of step 1 to produce reliable deployment for two bays. Consider bay combinations 3, 4, and bay 5, 6 in these studies.

3. Modify the results of step 2 to produce reliable deployment of four bays. Consider bays 3, 4, 5, 6 in this step since all values of link properties are included in this series of bays.

4. Verify the results of step 3 in a full 10-bay simulation.

3.0 RESULTS

This section presents preliminary results obtained using the analysis presented in section two. Possible deployment problems are identified and some "fixes" are proposed to improve dynamic performance.

3.1 ASSUMED CONDITIONS

The dynamics of the SASP deployable structure test article was analyzed for the deployment phase using the following assumed conditions:

1. Deployment is in the horizontal plane. Gravity neither promotes nor hinders deployment.

2. Link properties used are those calculated from detail design drawings. Numerical values are tabulated in Table 1.

3. A constant turning resistance of 5.0 lb-in/joint is assumed for all joints.

4. Coulomb and viscous damping in the telescoping members are neglected.

5. Utility cable loading is neglected.

6. Deployment cable haul-in rate is 0.375 in/sec.

7. The deployment cable haul-in winch is assumed to be powerful enough to maintain the specified haul-in rate regardless of load.

8. The 3/16 inch diameter deployment cable is considered to have an effective modulus of elasticity of 12×10^6 psi. The cables are treated as two springs in parallel.

9. No break-out springs or other augmentation of the cable deployment system is provided.

3.2 PRELIMINARY FINDINGS

Analysis using the above conditions lead to the following preliminary results:

1. For the fully compacted structure (i.e., $\theta_r = 90°$ or $270°$, $1 \leq r \leq 10$), forces generated by the cable deployment system will not produce deployment motion. This is because this is a singular configuration of the linkage in which links become parallel and aligned. Hence, some additional deployment mechanism will be necessary to "break" the linkage out of this configuration.

2. If the linkage is broken out slightly (i.e., $\theta_r = 89.9°$, or $270.1°$, $1 \leq r \leq 10$), the linkage will deploy. However, the simulation predicts that significant periods of slack deployment cable ($P_c = 0$) will occur. The slack cable condition results from the initially high cable tensions that develop due to the poor deployability of the linkage in its compacted mode. This initially high tension produces accelerations which eventually lead to link velocities in excess of the haul-in rate of the winch and the cables go slack. The linkage then coasts until joint resistance slows it down to the point where the cables again take load and the process repeats itself. This phenomena is illustrated by plots of P_c and θ_r versus time for various starting positions ($\theta_0 = 89.9°$, $89°$, $85°$) as shown in Figure 8. Since the results of slack cable (i.e., jamming, derailment of the cable from pulleys, failure due to impact loading, etc.) have not been modeled, the slack cable condition ($P_c = 0$) is treated in

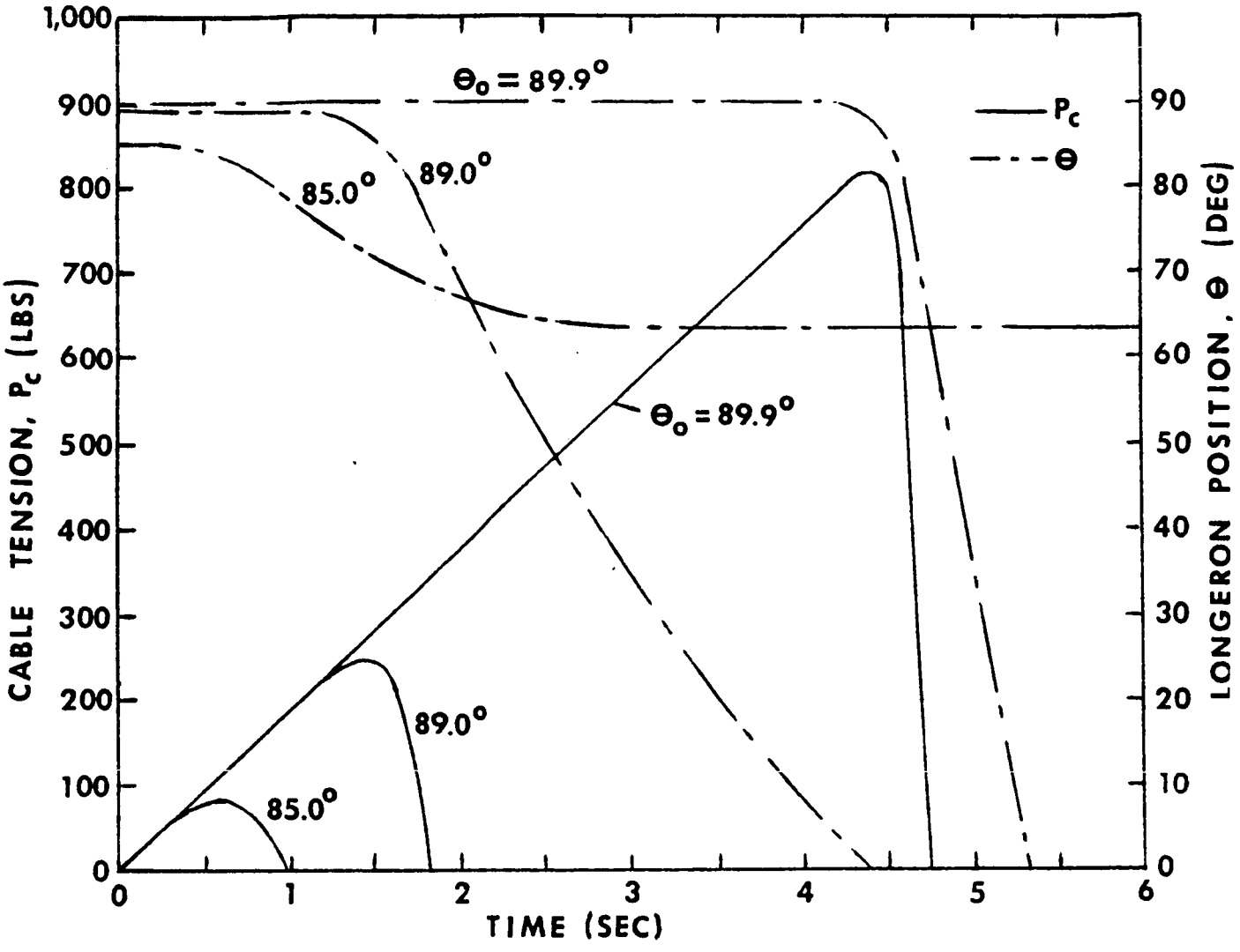

Figure 8. Variation of deployment cable tension (P_c) and longeron position (θ_r) with time for various initial positions (θ_0). Data is for Bay 6 with T_{joint} = 5.0 in.lb.

this study as a failure to deploy condition. Hence, for the conditins of this analysis, it appears likely that some deployment difficulty will be experienced for the SASP test article as currently designed.

These are preliminary findings since there is no certainty that the simplified model used is truely representative of the actual hardware. For example, the winch capability implied by assumption 7 above is partly responsible for the slack cable condition predicted by the analysis. Since details of the drive system were not available for use in this study, this assumption, may in fact, be highly misleading. In order to check the assumptions, a sensitivity

study was conducted using a single-degree-of-freedom analysis. This lead to the following conclusions.

1. Variations of joint resistance up to three times the nominal value of 5.0 in-lb/joint produced little reduction in the tendency for the cable to go slack. This finding implies that variations in joint resistance will probably not effect dynamic performance appreciably.

2. Viscous damping in the telescoping members is a highly effective means for controlling the dynamic behavior of the linkage. Damping factors of 40 lb-sec/in or better were found to eliminate the slack cable condition for a one-degree-of-freedom system.

3. Utility cable drag helps to stabilize deployment. Values of X_{util} and Y_{util} on the order of 100 lbs. will eliminate the slack cable condition for a one-degree-of-freedom system. Unfortunately, deployment cable tensions must be quite high in order to overcome the cable drag.

4. Reducing the maximum force which can be developed by the deployment winch reduces the tendency for slack cable to occur. However, for $270 \leq \theta_r \leq 280$ or $80° \leq \theta_r \leq 90°$, the drive stalls when the cable tension is limited sufficiently to prevent the development of slack cable. Hence, some additional deployment mechanism is required.

3.3 DESIGN MODIFICATIONS

It is apparent from the findings of this study that some design modifications may be necessary to ensure reliable deployment of the SASP test article. Specifically, it appears that some augmentation of the deployment system is needed to break the linkage out of its fully compacted configuration. As is

shown in ref. [6], the most effective means for producing deployment of the SASP test article design when fully compacted is to apply a torque to the longeron links. Accordingly, it is suggested that torsional springs be provided on each longeron link to assist the deployment of the linkage over the range $270 \leq \theta_r \leq \theta_{e1}$, and $\theta_{e2} \leq \theta_r \leq 90°$. As described in section 2.4, provisions for torsional break out springs have been included in the model.

Assuming cable slack to be an undesireable condition, it appears that design modifcations which improve control over link motion is needed. Ideally, the possibility for unconstrained deployment which exists in the present design should be eliminated. One means for doing this is suggested by the 1-4-AAD-2 Design Concept depicted in Figure 5b of ref. [6]. In this approach, unconstrained deployment is prevented by controlling tension in a second cable system which forms diagonals running cross-wise to the telescoping links. It is felt that the addition of such a control cable to the present design would be a relatively easy modifcation to implement since it would only require the attachment of one pulley to each coupler link.

A second modification is to convert the telescoping links into viscous dampers. This would effectively control the linkage dynamics, however, implementation of this modifcation would probably be expensive. Also, the design problem of providing viscous damping in space may prove difficult. Testing of this concept showed that values of ζ_D = 40 lb-sec/in., K_{brk} = 50 in. lbs/sec and θ_e = 80° produced reliable, slack free deployment for a single degree-of-freedom system. Maximum cable tension for this condition was 87 lbs/cable.

Limiting cable tension via a slip clutch or equivalent may be the simplest modification available. Use of torsional breakout springs will prevent the stalled drive condition noted previously. Experiments showed that cable tension limited to 10 lbs/cable (20 lbs total) combined with a torsional breakout spring rate of 35 lb-in/rad and $\theta_{e1} = 280°$, $\theta_{e2} = 80°$ provided reliable deployment of the four degree-of-freedom system formed by bays 3, 4, 5, 6.

4.0 CONCLUSIONS AND RECOMMENDATIONS

A dynamic analysis of the deployment behavior of the SASP deployable structure test article design has been developed. The equations of motion are derived based upon the principle of virtual work and are integrated numerically using a digital computer. Analysis using the computer simulation is found to give results which make sense physically and are consistent with the conditions assumed. In general, the deployable linkage design is found to operate and behave as expected. It is noted that some augmentation of the deployment scheme may be needed to assist deployment when the structure is fully compacted. Also, the analysis indicates that periods of slack deployment cable are likely to occur during deployment of the present design.

In general, modeling of forces has been kept as simple as possible in keeping with preliminary nature of this analysis. It is recommended that the modeling of forces be improved to better reflect the actual loading conditions as knowledge of these conditions become better understood through laboratory testing of the full scale hardware. Specifically, further attention needs to be paid to the modeling of the deployment cable take-up drive and to the utility cable loads acting on the structure during deployment. Also, accuracy of the simulation can be no better than the physical data used. Hence, it is recommended that the various link properties (m_i, J_i, g_i) used in the simulation be experimentally determined using the actual hardware involved.

Usefulness of the analysis is somewhat limited due to the excessive computer time required for multi-bay simulations. It is shown that this problem can be partially bypassed by using a combination of single-degree-of-freedom

analysis and multi-degree of freedom analysis. However, there is no doubt that usefulness of the simulation would be greatly enhanced if the computer time limitation were reduced. To this end, it is recommended that further work aimed at increasing the computational efficiency of the algorithms used be conducted.

Finally, this analysis has shown the SASP deployable structure test article, as presently designed, to have a single, overriding deficiency with regard to its "deployability". That is, it is possible for the linkage to deploy in an unconstrained (uncontrolled) mode. This condition occurs whenever the combined velocities of all the telescoping links exceeds the haul-in rate of the deployment cable. Hence, the design problem becomes one of balancing resistance to motion within the structure against the deploying forces acting to produce deployment motion such that the unconstrained deployment (slack deployment cable) condition doesn't occur. The analysis has shown that this balance is precarious at best. Hence, it is recommended that the design modification suggested in this report as well as others be carefully considered so that "acceptable fixes" for this design deficiency be available should the need for them arise.

References

1. Greenwood, Donald T., Principles of Dynamics, Prentice-Hall, 1965

2. Paul, Burton, Kinematics and Dynamics of Planar Machinery, Prentice-Hall, 1979

3. System/360 Scientific Subroutine Package, Version III, Programmer's Manual, Doc. GH20-0205-4, IBM Technical Prod. Dept., White Plains, NY

4. Hamming, Richard W., Numerical Methods for Scientists and Engineers, McGraw-Hill, 1962

5. James, M.L., Smith, G.M., Wolford, J.C., Applied Numerical Methods for Digital Computation, 2nd Ed., Harper and Row, 1977.

6. Stoll, H.W., "Deployable Structure Design for the Science and Applications Space Platform", 1980 NASA/ASEE Summer Faculty Fellowship Program, Marshall Space Flight Center and the University of Alabama, NASA CR-161511, October 1980